ISSN (Print) 1226-1750
ISSN (Online) 2233-6656
Journal of Magnetics 26(4), 448-455 (2021) https://doi.org/10.4283/JMAG.2021.26.4.448

Analysis of Constituent Elements and Brownian Motion of the Conjugates of anti-CD3 Antibody and Magnetic Nanoparticles

Jong-Gu Choi, Ji-Won Ha, Sang-Heon Choi, Hyunsook Lee, and Sang-Suk Lee*

Department of Digital Healthcare, Sangji University, Wonju 26339, Republic of Korea

(Received 15 October 2021, Received in final form 4 December 2021, Accepted 10 December 2021)

An Fc-directed conjugate (mAb-MNP) of the anti-CD3 monoclonal antibody (mAb), Foralumab, and the surface amino groups on magnetic nanoparticles (MNPs) was prepared using the SiteClick antibody labeling kit. The conjugate was imaged by transmission electron microscopy and analyzed using energy dispersive spectrum and a nanoparticle tracking analyses. The average values of drift velocities (pix/frame) due to the Brownian motion of MNPs and mAb-MNPs in phosphate-buffered saline were 3.16/0.76 and 6.70/1.98 on the x-/y-axes, respectively. Two different hydrodynamic diameters of 180.0 nm and 258.8 nm were found for the MNPs and the mAb-MNPs with an actual size of 35 nm, respectively. The drift velocity was 2 times (2×) higher for mAb-MNPs than MNPs in proportion to the 2× higher value of the square of the hydrodynamic diameter of the conjugate relative to the MNPs as calculated by Stokes' law. Thus, the conjugates of Foralumab with MNPs have better fluidity in PBS than free MNPs.

Keywords : Foralumab, magnetite, mapping image, brownian motion, drift velocity, Stokes' law

1. Introduction

Magnetic nanoparticles (MNPs) have received much attention due to their wide applicability for the separation of cells, genetic cloning, biosensors, and magnetic resonance imaging (MRI) for biomolecular diagnosis and other biological applications [1, 2]. Of note, MNPs are being commercialized for use in various biochemical separation and refining techniques. Generally, tens-of-nanometer-sized MNPs with a superparamagnetic property have been used to effectively separate or refine DNA, proteins, and peptides by bonding to biomolecules [3, 4]. MNPs, which are magnetic iron oxides, are largely composed of two types of polymorphic forms-magnetite (Fe_3O_4) and maghemite (γ-Fe_2O_3). MNPs have a core-shell structure and are used to modify the surface of various types of biological substances (*e.g.*, carbon-hydrates, polymers, lipids, proteins) [5, 6]. Recently, MNPs with a core-shell structure composed of ferrite oxide and zinc oxide have been used to help monitor the movement and effectively improve the delivery of dendritic cells using MRI and through the incorporation of tumor-specific antigens on the surface of MNPs [7].

There are seven types of corona viruses, of which SARS-CoV-2 is the cause of the serious, ongoing, global coronavirus disease 2019 (COVID-19) pandemic. When SARS-CoV-2 invades the human body, the oversecretion of cytokines by the immune system plays an important role in the host response [8, 9]. Indeed, cytokine release syndrome (CRS) involving T cells is known to be one of the leading causes of death due to COVID-19 [10, 11]. Treatments include cytokine receptor inhibition, specific immune cell depletion, and steroid hormones. Monoclonal antibody (mAb) treatment involves the depletion of specific immune cells to inhibit cytokine secretion by inhibiting cluster of differentiation 3 (CD3), an important signaling molecule for the activation of T cell receptors (TCRs) [5].

To combat CRS, targeted immunotherapy must be developed to deliver a proper amount of anti-CD3 mAb via the blood circulation to the site of inflammation. Therefore, this study aimed to conjugate anti-CD3 mAbs to MNPs to deliver the antibodies as immunotherapy and analyze the structure of the conjugate using transmission electron microscopy (TEM) and energy dispersive spectral (EDS) mapping. Brownian motion of MNPs in phosphate-buffered saline (PBS) was investigated using a nanoparticle tracking analyzer (NTA) to investigate the properties of

©The Korean Magnetics Society. All rights reserved.
*Corresponding author: Tel: +82-33-730-0415
Fax: +82-33-738-7610, e-mail: sslee@sangji.ac.kr

© 2021 Journal of Magnetics

the conjugate's flow in fluid.

2. Structure and Function of the anti-CD3 Monoclonal Antibody

Anti-CD3 mAb binds to CD3 in the TCR complex and inhibits cytokine storms in three ways. First, when the antibody binds to the receptor, it removes the receptor from the cell surface, preventing T cell activation. The antibody can be dislodged by shedding or is internalized and absorbed. Second, if the antibody binds to an activated T cell, it induces anergy–a state in which no immune reaction occurs even when an antigen is injected into the body. Anergy leads to T cell inactivation via the release of cytotoxic T lymphocyte antigen-4 (CTLA-4) to the surface. Third, anti-CD3 mAb binding to the TCR induces the secretion of the cytokine, transforming growth factor-beta (TGF-β), leading to T cell apoptosis. TGF-β induces forkhead box P3 (FoxP3) activation in regulatory T cells (Tregs) and Treg differentiation, leading to the production of tolerogenic dendritic cells (DCs) and contributing to suppression of the immune response, including that of effector T cells [13].

The anti-CD3 mAb used in this study is a 100 % humanized anti-CD3 epsilon therapeutic antibody called 'Foralumab,' which was first developed by Tiziana Life Sciences [14] and later manufactured by Creative Biolab [13]. This product is for research use only and is not intended for diagnostic use. As a recombinant monoclonal antibody against CD3 epsilon, Foralumab is an immune-modulator that binds to CD3 epsilon. The CD3-epsilon polypeptide, together with CD3-gamma, -delta, and -zeta, and the TCR alpha/beta and gamma/delta heterodimers, forms the TCR–CD3 complex. This complex plays an important role in coupling antigen recognition to several intracellular signal transduction pathways. The genes encoding the epsilon, gamma, and delta polypeptides are located in the same cluster on chromosome 11. The epsilon polypeptide plays an essential role in T cell development. Defects in this gene cause immunodeficiency and are linked to a susceptibility to type I diabetes in women [13]. Fig. 1(a) shows the hypothetical 3D structure of Fc-directed Foralumab as an anti-human CD3 epsilon therapeutic antibody with a size of 5-8 nm. The 2D structure of Foralumab includes the Fc region with a heavy chain and Fab regions with two light chains and antigen binding sites, as shown in Fig. 1(b). Eight sulfur (S) atoms are linked in disulfide bonds between one heavy chain and two light chains of the antibody.

3. Properties of MNPs and Conjugation of mAb and MNPs

The superparamagnetic MNPs used in this study (Fig. 2(a)) (nanoComposix SCM0067, San Diego, USA) are aminated, silica-shelled magnetite (amine-SiO_2-Fe_3O_4) with amine groups attached to the surface [15]. Transmission electron microscopic (TEM) images of these MNPs taken with the JEOL 1010 TEM are shown in Fig. 2(b), Fig. 2(c), and Fig. 2(d). The average diameter of one

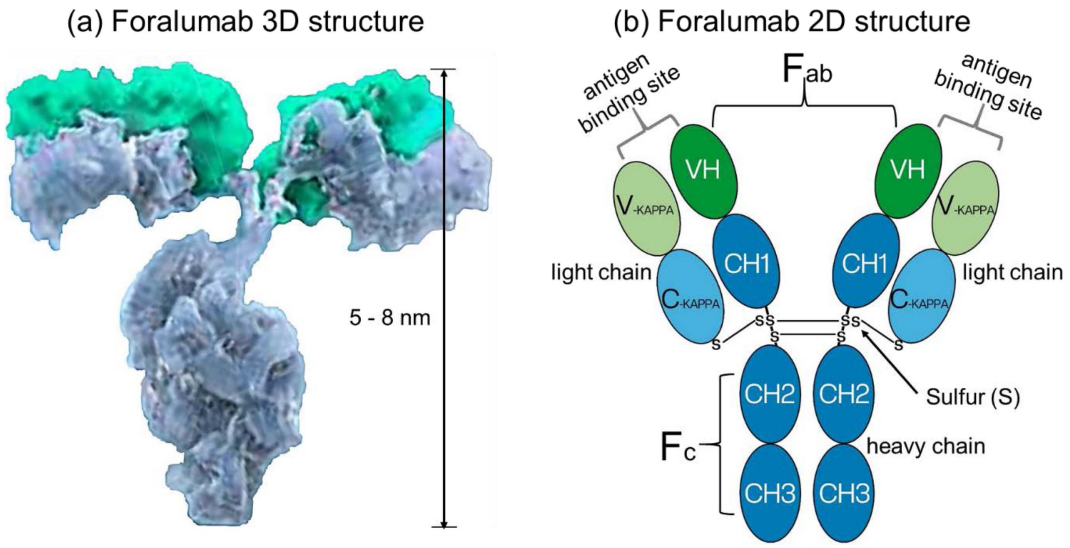

Fig. 1. (Color online) (a) Hypothetical 3D structure of Fc-directed Foralumab as anti-human CD3 epsilon therapeutic antibody with a size of a few nm. (b) Schematic diagram of 2D structure including the Fc region with a heavy chain and Fab regions with two light chains and antigen binding sites. The eight sulfur (S) atoms linked via disulfide bonds between one heavy chain and two light chains.

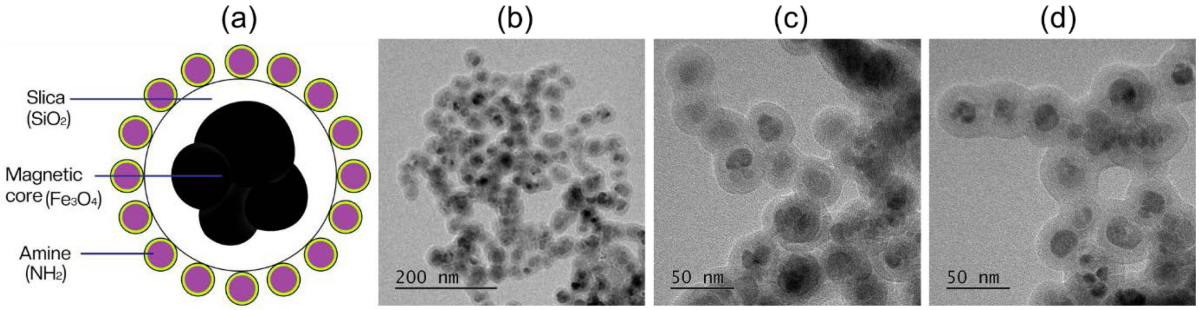

Fig. 2. (Color online) (a) Structure of one aminated silica-shelled magnetite (Fe_3O_4). (b), (c), and (d) TEM photos of amine-SiO_2-Fe_3O_4 nanoparticles (nanoComposix) with surface area of diameter ~ 33 ± 5 nm and aminated particle surface [15]. Scale bars: (b) 200 nm, (c) and (d) 50 nm.

MNP with Fe_3O_4 in the core and an even coating of the protective silica layer is 33 ± 5 nm. The suspension of MNPs in distilled water (DW) had a pH of 5.2 and a concentration of 3.12 mg/mL. The hydrodynamic diameter was 249.3 nm, and the zeta potential was 40.2 mV [15]. MNPs should be shaken vigorously before use, sonicated if needed, and stored at 2-8 °C without freezing.

As shown in Fig. 3, the mAb-MNP conjugate is prepared using the SiteClick^{TM} antibody labeling kit manufactured by ThermoFisher (USA), so that the antibody is

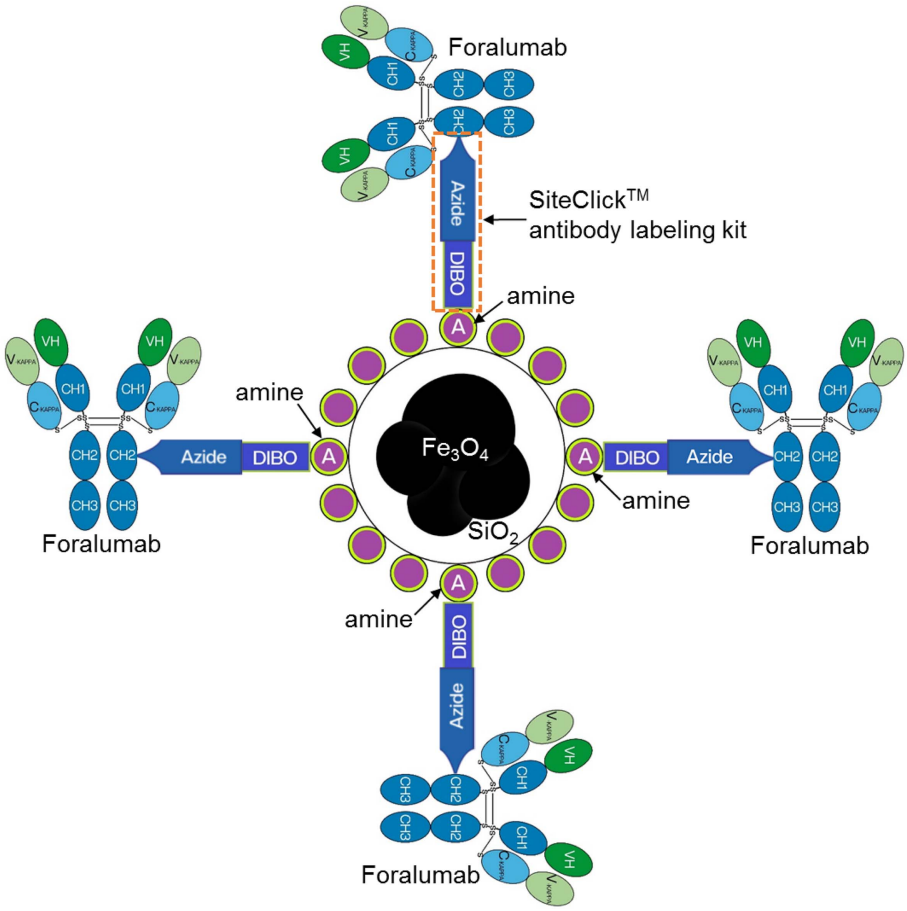

Fig. 3. (Color online) The schematic diagram of conjugation between monoclonal antibody-azide-DIBO and the amino group on the surface of magnetic nanoparticles. Anti-CD3 mAbs conjugated to MNPs via Fc-directed conjugation. The Click-iT™ sDIBO Alkyne for SiteClick™ Antibody Labeling kits are designed to be used with the SiteClick™ Antibody Azido Modification Kit or with engineered antibodies containing azide moieties [16]. Scale bars: (a) and (e) 50 nm, (b)-(d) and (f)-(h) 100 nm

Fc-directed and conjugated to the surface of MNP via an amine group [16]. T cell activation is achieved only when the MNP-conjugated antibody simultaneously binds to the two receptors, CD3 and CD28, in the TCR on the surface of the T cell [17]. The experimental procedure for conjugation of the anti-CD3 mAb, Foralumab, to MNPs with amine functional groups is performed sequentially from steps 1 to 7 described below, according to the SiteClick^{TM} antibody labeling workflow [16]: Step 1: antibody concentration and buffer exchange; Step 2: modifying the carbohydrate domain of the antibody; Step 3: attaching azide to the antibody; Step 4: purification and concentration of the modified azide-antibody; Step 5: dibenzocyclooctyne (sDIBO) label-binding process; Step 6: purification and concentration of the antibody conjugate. Step 7 is the final process of binding the mAbs to MNPs; a suspension of MNPs with an amine functional group in DW is exchanged with a buffer of 1× Tris-buffered saline (TBS) or PBS so that the particle concentration is 1 mg/mL. The azide-sDIBO attached to Foralumab, the final modified anti-CD3 mAb obtained through step 6, is added to the MNP suspension. In general, as shown in Fig. 3, when an antibody is attached to MNPs, its Fc region, rather than the Fab region, must be bound to the MNPs for the elimination of side effects in immunotherapy.

4. TEM Images and Properties of the Conjugates of anti-CD3 mAbs and MNPs

The surface structure of MNPs with free amine groups was analyzed using field emission TEM (JEM-F200, JEOL Ltd, Japan). Spatial resolution and analysis performance were improved for multipurpose analysis, and high resolution was provided with a user-centered integrated control system. Amount enough to coat the NMPs powder on the mesh was loaded on the TEM grid, and TEM and rapid EDS mapping analyses were performed for the two samples (MNP and mAb-MNP) [18]. Immediately after analyzing the TEM images, the bonding elements were investigated using EDS mapping. The main constituent elements of MNPs are Fe and O (Fig. 2(a)), whereas S is the main element of interest of Foralumab (Fig. 1(b)).

Fig. 4(a) is a TEM image of MNPs on a grid after removing moisture from a suspension in DW. The diameter distribution of MNPs is within the range of 25-35 nm. When an electron beam is incident on the amine group on the surface of the MNPs, Characteristic x-rays are emitted as the outer electrons of the atom transition to the positions of the vacant central orbital electrons. The observed image, Fig. 4(b), is a TEM image of the thin solid electrolyte interphase (SEI) layer caused by the electrode-electrolyte interface reaction [19]. Fig. 4(c) shows the characteristic x-rays emitted from Fe in MNPs, while Fig. 4(d) shows the characteristic x-rays emitted from S in the center of the Foralumab antibody. No x-rays due to S are seen in the case of free MNPs.

Fig. 4(e), Fig. 4(f), Fig. 4(g), and Fig. 4(h) are images

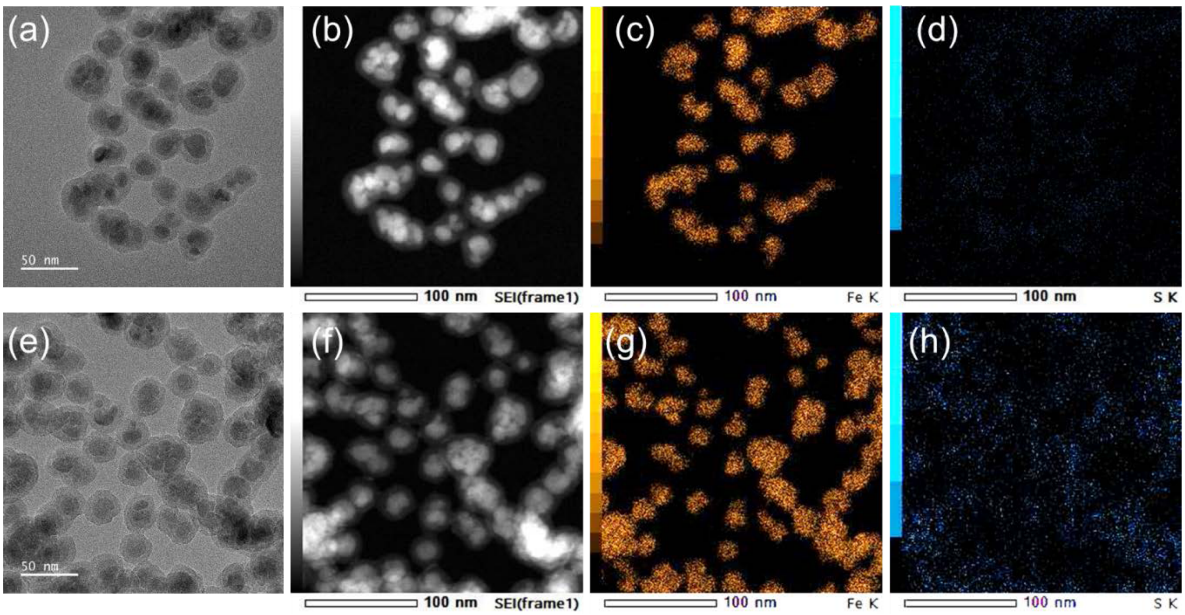

Fig. 4. (Color online) Images of transmission electron microscope (a) and atomic intensities of (b) SEI, (c) Fe, and (d) S for elements of aminated, silica-shelled magnetite (Fe_3O_4) MNPs with a diameter of 25-35 nm. Images of TEM (e) and atomic intensities of (f) SEI, (g) Fe, and (h) S for elements of mAb-MNPs (anti-CD3 Foralumab mAb-azide-DIBO-MNPs of aminated, silica-shelled magnetite) with a diameter of 25-40 nm.

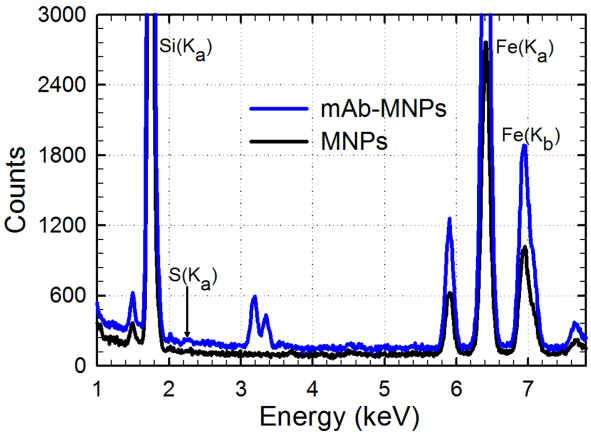

Fig. 5. (Color online) The EDS spectrum of amine-SiO_2-Fe_3O_4 (MNPs, black line) and Foralumab-azide-DIBO-amine-SiO_2-Fe_3O_4 (mAb-MNPs, blue line) to analyze their atomic stoichiometric characteristics. S and Fe are the major elements constituting the framework of the Foralumab mAb-MNPs. The characteristic energies for the S and Fe elements are 2.307 keV and 6.498 keV, respectively.

of the conjugates of the anti-CD3 mAbs and MNPs. Although there seems to be no clear difference in surface topography between free MNPs and mAb-MNPs, their diameters are different. These characteristics could have a significant impact on flow characteristics of the Foralumab antibody attached to the MNPs. Fig. 4(e), 4(f), and 4(g) show the TEM images of the SEI layer and the atomic intensities of the SEI layer and Fe element, respectively. The main constituent elements of mAb-MNPs, which can be distinguished from MNPs, are shown in Fig. 4(h), with characteristic x-rays being emitted from S. The sky-colored image shown in Fig. 4(h) confirms the characteristic x-ray image emitted from S in the center of the Foralumab antibody conjugated to MNPs.

The EDS spectrum obtained from elemental intensity analysis by TEM is shown in Fig. 5. The blue peaks of the mAb-MNP conjugates overlap many black peaks corresponding to free MNPs. Here, S and Fe are the main elements constituting the framework of the Foralumab antibody and the core of the MNPs, and the characteristic energies of S and Fe are 2.307 keV and 6.498 keV[20], respectively. In particular, it can be seen that the blue peaks of mAb-MNPs have generally higher count values than the black peaks of MNPs. In Fig. 5, the EDS peak of element S indicated by an arrow at 2.307 keV was higher for mAb-MNPs than for MNPs. Thus, the results of the EDS analysis shown in Fig. 5, similar to the results shown in Fig. 4, confirmed that the Foralumab antibody was conjugated to the MNPs.

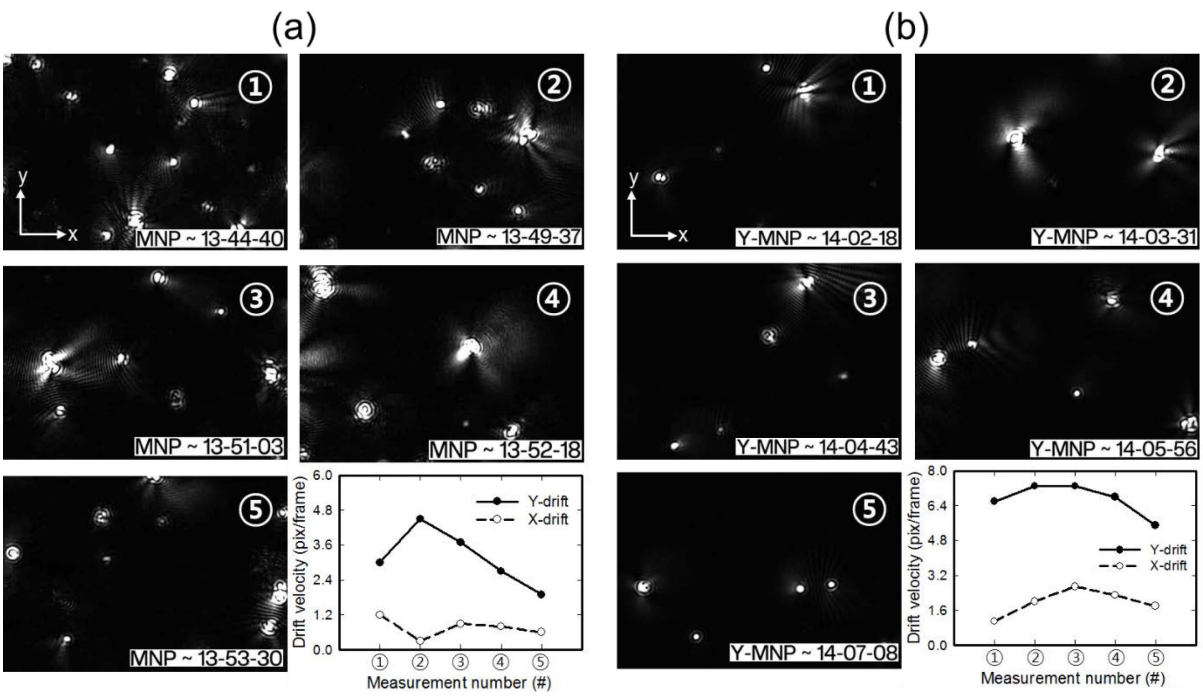

Fig. 6. Single shots of flow images and analyses of Brownian motion obtained by NTA device in 5 different groups of MNPs and mAb-MNPs samples immersed in 1× PBS at a concentration of 1 μg/mL. Several white spots seen on the black screen are the positions of the nanoparticles during motion. Here, the drift velocity of all particles is calculated from motion images and expressed in units of pix/frame. The mean x-axis and y-axis drift velocities calculated by two inset sixth graphs are +3.16 pix/frame, 0.76 pix/frame and +6.70 pix/frame, +1.98 pix/frame for (a) MNPs and (b) mAb-MNPs, respectively.

5. Analysis of Brownian Motion and Application of Stokes' Law for mAb-MNP Conjugates

Next, we examined the size distribution MNPs and mAb-MNPs in liquid and their Brownian motion [21, 22]. Brownian motion is observed when molecules or atoms in a liquid or gas collide with small particles, causing the particles to move irregularly. To observe Brownian motion, we used an NTA (Malvern Panalytical, Model: NanoSight NS300, Malvern, United Kingdom) device, which visualizes and analyzes particle characteristics based on light scattering and Brownian motion velocity related to particle size [23]. When a laser beam passes through a liquid sample chamber containing particles, the particles in the path of the beam scatter light and the drifting Brownian motion of the particles can be visualized as an image with a 200× magnification microscope equipped with a camera. MNPs and mAb-MNPs were suspended in DW or PBS to prevent aggregation between the particles due to the charges of the functional groups attached to the surface without the external magnetic field. The speed of the particle movements due to Brownian motion was not affected by particle density or refractive index and was only related to the viscosity and temperature of the liquid; hence, the suspension was kept the constant viscosity and the room temperature [24].

As seen in Fig. 6(a) and Fig. 6(b), NTA [24] was performed for five groups of each sample of MNPs and mAb-MNPs at a concentration of 1 μg/mL in 1× PBS. Fig. 6(a) and Fig. 6(b) are screen captures showing the Brownian motion of the MNPs and the mAb-MNP conjugates. The drift velocity of all particles in PBS was calculated from the motion images and converted into pix/frame units. The Brownian motion of MNPs for the five images was summarized numerically in the lower graph of Fig. 6(a) by separating the average velocity of each group in the x-axis and y-axis directions. The average values of the x-axis and y-axis movement speeds were +3.16 pix/frame and 0.76 pix/frame, respectively. The average speeds of Brownian motion of mAb-MNPs were +6.70 pix/frame and +1.98 pix/frame along the x-axis and y-axis directions, respectively, as shown in the lower graph of Fig. 6(b). These results indicate that the speed of Brownian motion of mAb-MNP conjugates was more than twice that of free MNPs.

As shown in Fig. 6(a) for the movement of MNPs in PBS, the effective value calculated from the average values in the x-axis and y-axis directions is 3.25 pix/frame, and the direction is toward the northeast. As shown in Fig. 6(b) for the movement of mAb-MNPs, the effective value calculated from the average values in the x-axis and y-axis directions is 6.98 pix/frame, and the direction is toward the northeast. Thus, the results of Brownian motion analysis show that mAb-MNPs move about twice as fast as free MNPs, indicating that the anti-CD3 antibody, Foralumab, attached to the surface of MNPs showed a faster migration rate in PBS than free MNPs. Thus, the larger the radius is, the faster the particle flows in proportion to the square of its radius. The hydrodynamic radius is obtained by applying Stokes' law on the resistive force received by the particles from the fluid, and its value is higher for mAb-MNPs than for MNPs [24, 25].

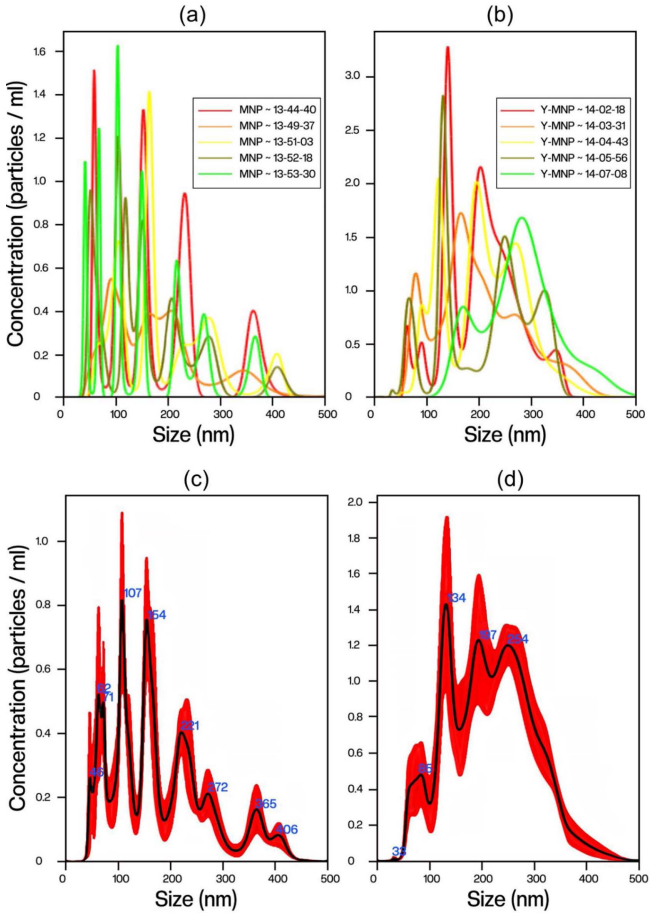

Fig. 7. (Color online) Finite track length adjustment (FTLA) Concentration versus Size graphs for NTA analysis of (a) MNPs and (b) mAb-MNPs. Averaged FTLA Concentration versus Size graphs for NTA analysis of (c) MNPs and (d) mAb-MNPs. (a) Mean concentration ± Standard error (S.E.): $8.96 \times 10^7 \pm 4.89 \times 10^6$ particles/mL and mean size ± S.E.: 180.0 ± 4.7 nm. (b) Mean concentration ± S.E.: $2.63 \times 10^7 \pm 1.18 \times 10^6$ particles/mL and mean size ± S.E.: 258.8 ± 14.2 nm.

If the particle is large, the force is canceled because the force is almost uniform on all sides. In the case of non-

moving, nano-sized particles, they collide disproportionately and "wander around." According to the law that defines the resistance force that occurs when moving in a fluid at rest, the resistance of the fluid is proportional to the moving speed and the radius of the spherical particle. If an object is moving with acceleration in a fluid, its terminal velocity is reached when the resistive force equals the accelerating force. The terminal velocity can be obtained as follows by applying Stokes' law [26, 27].

$$V_s = \frac{2}{9}\frac{r^2 a(\rho_p - \rho_f)}{\eta} \quad (1)$$

Here, V_s is the particle's terminal velocity (m/s), r is the particle's Stokes radius (m), a is the motional acceleration of the particle in the fluid (m/s^2), ρ_p is the particle's density (kg/m^3), ρ_f is the density of the fluid (kg/m^3), and h is the viscosity coefficient of the fluid (Pa·s). The radius r of Stokes given in Eq. (1) above can be estimated as the hydrodynamic size observed through a nanoparticle tracker that can measure the size of particles moving by Brownian motion.

Fig. 7 shows the concentration (number of particles/mL) distribution by finite track length adjustment (FTLA) according to each size obtained from the Brownian motion image analyzed in Fig. 6 [28]. From the data collected for each of the five groups, it can be seen that the hydrodynamic diameter of mAb-MNPs is larger than that of MNPs. Fig. 7(a) and 7(c) show the concentration distribution according to the particle size for MNPs: the mean concentration ± standard error (S.E.) = $8.96 \times 10^7 \pm 4.89 \times 10^6$ particles/mL, mean size ± S.E. = 180.0 ± 4.7 nm. Fig. 7(b) and 7(d) also show the concentration distribution according to the particle size for mAb-MNPs: mean concentration ± S.E. = $2.63 \times 10^7 \pm 1.18 \times 10^6$ particles/mL, mean size ± S.E. = 258.8 ± 14.2 nm. Fig. 8(a) and 8(b) show the intensity in particle strength with particle size, which supports the abovementioned data.

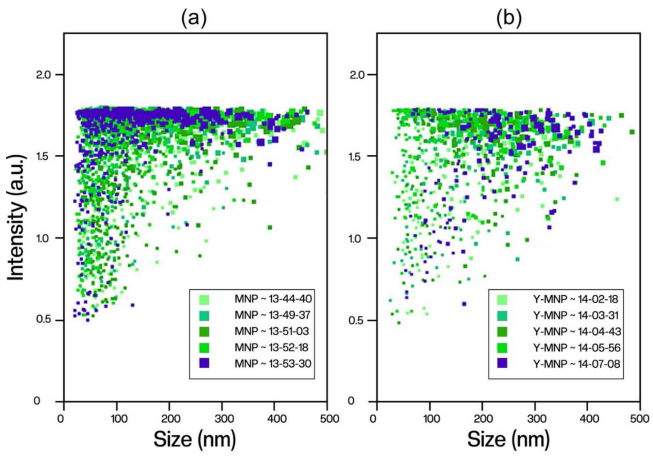

Fig. 8. (Color online) Intensity versus Size graphs for NTA analysis of (a) MNPs and (b) mAb-MNPs.

The average values of MNPs and mAb-MNPs obtained from the data of concentration and intensity distribution analyzed by NTA are 180.0 nm and 258.8 nm, while their radii are 90.0 nm and 129.4 nm, respectively. As the square of the radius is proportional to the flow rate, $(129.4)^2/(90)^2 = 2.06$, which is consistent with the almost 2× the difference in drift velocities observed between mAb-MNPs and free MNPs.

6. Conclusions

An optimal Fc-directed conjugate of Foralumab with the amine group-containing MNPs was prepared–mAb-MNPs–using the SiteClick antibody labeling kit, which provides instructions for an antibody control, buffer exchange, antibody carbohydrate domain modification, azide attachment, and azide-modified antibody purification and concentration procedures. The mAb-MNP conjugate was confirmed by observing TEM images and EDS maps, including those of S elemental spectra and images. The average values of drift movement speed due to Brownian motion of MNPs and mAb-MNPs in PBS were measured as +3.16 pix/frame, 0.76 pix/frame on the x-axis and +6.70 pix/frame, +1.98 pix/frame on the y-axis, respectively. Particle size, concentration distribution, and intensity distribution were analyzed by NTA for MNPs and mAb-MNPs with an actual size of 35 nm. The hydrodynamic diameter was found to be 180.0 nm and 258.8 nm on average for MNPs and mAb-MNPs, respectively. The 2× increase in drift velocity for mAb-MNPs could be attributed to Brownian motion in proportion to the higher value for the square of the radius of the conjugate according to Stokes' law. These results show that the conjugate of the anti-CD3 antibody, Foralumab, with MNPs has suitable fluidity in PBS. In addition, in the use of MNPs conjugated with mAbs, a simple microneedle liquid patch can be attached to the skin to obtain injection efficiency, and an immunotherapeutic agent can be induced by attaching it to a target site. It is considered that the treatment effect can be maximized by reducing the burden on the patient and providing a sense of stability. The mAb-MNPs still migrate easily to sites of virus entry, making this conjugate useful for treating CRS in COVID-19 cases.

Acknowledgments

This research was supported by Basic Science Research Program through the National Research Foundation of Korea (NRF) funded by the Ministry of Education

(2021R1I1A3054773).

References

[1] A. E. Mengesha, R. J. Wydra, J. Z. Hilt, and P. M. Bummer, Pharm. Res. **30**, 3214 (2013).
[2] A. Akbarzadeh, M. Samiei, and S. Davaran, Nanoscale Res. Lett. **7**, 144 (2012).
[3] K. S. Butler, D. M. Lovato, M. L. Adolphi, et al., Cell Transplantation **22**, 1943 (2013).
[4] V. F. Cardoso, A. Francesko, C. Ribeiro, et al., Adv. Healthcare Mater. **7**, 1700845 (2018).
[5] G. F. Goya, V. Grazu, and M. R. Ibarra, Curr. Nanosci. **4**, 1 (2008).
[6] J. H. Lee, J. T. Jang, J. S. Choi, et al., Nat. Nanotechnol. **6**, 418 (2011).
[7] N. H. Cho, T. C. Cheong, J. H. Min, et al., Nat. Nanotechnol. **6**, 675 (2011).
[8] H. Ledford, Nature **591**, 513 (2021).
[9] E. Callaway, Nature **580**, 576 (2020).
[10] S. Su, G. Wong, W. Shi, et al., Trends Microbiol. **24**, 490 (2016).
[11] S. F. Pedersen and Y. C. Ho, J. Clin. Invest. **130**, 2202 (2020).
[12] R. Channappanavar and S. Perlman, Semin. Immunopathol. **39**, 529 (2017).
[13] creative biolabs, https://www.creativebiolabs.net/foralumab-overview.htm
[14] Tiziana Life Sciences, http://www.tizianalifesciences.com/drug-pipeline/foralumab/
[15] NanoComposix, https://nanocomposix.com/collections/material-magnetite/products/biopure-magnetite-nanoparticles-pvp?variant=15906783264857
[16] Thermofisher, https://www.thermofisher.com/order/catalog/product/S20026#/S20026
[17] Humancells Bioscience, https://humancellsbio.com/products/human-cord-blood-cd3-pan-t-cells
[18] M. Kawasaki, T. Oikawa, K. Ibe, K. Park, and M. Shiojiri, J. Elec. Microscopy **47**, 335 (1998).
[19] S. J. An, J. Li, C. Daniel, D. Mohanty. S. Nagpure, and D. L. Wood, Carbon **105**, 52 (2016).
[20] B. Wang, K. Zhou, B. Wang, Z. Gui, and Y. Hu, Ind. Eng. Chem. Res. **53**, 12355 (2014).
[21] Brown motion, https://m.blog.naver.com/PostView.naver?isHttpsRedirect=true&blogId=miseos&logNo=220679417904
[22] J. R. Schmidt and J. L. Skinner JL, J. Phys. Chem. **B108**, 6767 (2004).
[23] Malvern Panalytical, https://www.malvernpanalytical.com/kr/products/technology/light-scattering/nanoparticle-tracking-analysis
[24] E. P. Hansen, B. Fromm, S. D. Andersen, A. Marcilla, et. al., J. Extracellular Vesicles **8**, 1578116 (2019).
[25] S. Ahmad, S. Sheriff, and M. Farooq, J. Magnetics **26**, 347 (2021).
[26] D. Nahshol, Am. J. Phys. **33**, 657 (1965).
[27] E. M. Wray, Phys. Educ. **12**, 300 (1977).
[28] A. Kim, W. B. Ng, W. Bernt, and N. J. Cho, Sci. Rep. **9**, 2639 (2019).